Applied Physics A (2018) 124:766
https://doi.org/10.1007/s00339-018-2195-z

Applied Physics A
Materials Science & Processing

Strong third-order optical nonlinearities of Ag nanoparticles synthesized by laser ablation of bulk silver in water and air

G. S. Boltaev[1] · R. A. Ganeev[1] · P. S. Krishnendu[1] · S. K. Maurya[1] · P. V. Redkin[1] · K. S. Rao[1] · K. Zhang[1] · Chunlei Guo[1,2]

Received: 31 July 2018 / Accepted: 16 October 2018 / Published online: 22 October 2018

Abstract
We demonstrate the correlation between strong nonlinear optical response of silver nanoparticles (Ag NPs) out of plasmon resonance and efficient third harmonic generation in the plasmas containing Ag NPs. The dynamics of nonlinear optical response of the 8 nm and 50 nm Ag NPs prepared by laser ablation of bulk silver in deionized water using 6 ns, 200 ps, and 60 fs laser pulses is systematically analyzed. Their optical limiting properties are studied at the wavelengths of 800 and 355 nm, using femtosecond and nanosecond laser pulses. Nonlinear absorption coefficient of 8 nm Ag NPs at the wavelength of 1064 nm was measured to be as high as 3×10^{-5} cm W^{-1}. Nonlinear refraction shows the change of sign with variation of the wavelength and duration of probe laser pulses. The theoretical calculation of silver ablation shows the formation of a few nanometer sized particles. We also analyze third harmonic generation in the laser-produced plasmas containing Ag NPs and attribute the enhancement of this process to the influence of small silver clusters. The conversion efficiency of 800 nm towards the third harmonic was measured to be 4×10^{-3}, which was a few times larger compared with similar process in air.

1 Introduction

The synthesis of nanostructured materials took much attention due to their advanced optical and nonlinear optical properties, which can be used in various area of communications, optics, laser physics and medicine [1, 2]. During last two decades, special attention was given to the nonlinear optical properties of the nanoparticles (NPs) of variable morphology [3, 4]. The attractive application of these nanostructured materials in optics is the protection of sensitive area of detection system through optical limiting (OL) of high-power laser radiation. One can anticipate that variations of the sizes of NPs can significantly enhance OL. In [5], the metal nanoparticle-embedded polymer film and their optical limiting capability were demonstrated. OL behavior of silver nanoparticles with different sizes and shapes is investigated and compared to the optical limiting performance of conventional carbon black suspension [6]. It found that the optical limiting effect is strongly particle size dependent and the best performance is achieved with the smaller particles.

Silver nanoparticles took special attention among numerous small-sized species due to their use in imaging, biosensors, photovoltaic devices, solar cells, light emitting devices, catalysis, etc. Silver nanoparticles (Ag NPs) have unique optical, electrical, and thermal properties and are already found applications being incorporated into products that range from photovoltaics to biological and chemical sensors. Examples include conductive inks, pastes and fillers which utilize Ag NPs for their high electrical conductivity, stability, and low sintering temperatures. Additional applications include molecular diagnostics and photonic devices, which take advantage of the novel optical properties of these nanomaterials. Ag NPs are extraordinarily efficient at absorbing and scattering light and, unlike many dyes and pigments, have a color that depends upon the size and the shape of the particle. The strong interaction of the Ag NPs with light occurs because the conduction electrons on the metal surface undergo a collective oscillation when excited by light at specific wavelengths. The advantages of Ag NPs include

✉ R. A. Ganeev
rashid_ganeev@mail.ru

✉ Chunlei Guo
guo@optics.rochester.edu

[1] The Guo China-US Photonics Laboratory, State Key Laboratory of Applied Optics, Changchun Institute of Optics, Fine Mechanics and Physics, Chinese Academy of Sciences, Changchun 130033, China

[2] The Institute of Optics, University of Rochester, Rochester, NY 14627, USA

monodisperse distribution in surrounding environment without agglomeration and aggregation, comprehensive characterization including TEM and UV–Vis, good stability and long life time. A unique property of spherical Ag NPs is that its surface plasmon resonance (SPR) can be tuned from 400 to 530 nm by changing the particle size and the local refractive index near the particle surface. Even larger shifts of resonance peak towards the IR region can be achieved by producing silver nanoparticles with rod or plate shapes.

Different physical and chemical techniques are used for the preparation of metallic NPs with variable morphology and sizes. Among them, laser ablation of bulk material has been proven to be a simple method for the synthesis of spherical Ag NPs in various liquids [7]. In many cases, the distilled water is used during laser ablation of silver. Laser ablation of silver was also performed in NaCl aqueous solution [8]. It was shown that the efficiency of Ag NPs formation depends on the concentration of NaCl in aqueous solution. Increase NaCl concentration up to some threshold values led to decrease of the probability of NPs aggregation. Preparation of NPs in various solutions has many applications. For example, Ag NPs prepared during ablation in water are useful for surface-enhanced Raman scattering spectroscopy [9, 10]. Preparation of colloidal Ag NPs in aqueous gelatin solution using nanosecond pulses of Nd:YAG laser at the wavelength of 532 nm was reported in Ref. [11]. They have shown the influence of the pulse repetition rate on the morphology and optical properties of samples. Synthesis of Ag NPs in ethanol by laser ablation using photoacoustic pulsed technique was reported in Ref. [12]. The application of photoacoustic technique allowed controlling the production rate per laser pulse, and the concentration of synthesized Ag NPs.

Modification of Ag NPs size distribution by laser irradiation of their water suspensions was reported in Ref. [13]. The change of the nanoparticles' characteristics caused by variable laser fluence and duration of irradiation was observed. A considerable narrowing (by a factor of three) of the SPR bandwidth was achieved, which is the evidence of narrowing of the particles size distribution. Time-dependent preparation of gelatin-stabilized Ag NPs was demonstrated in Ref. [14]. The mean diameter of Ag NPs decreased with increasing the ablation time of silver target. Ag NPs with sizes of 8 nm have been synthesized in ethanol [15]. The SPR of these NPs have shown maximum absorption at 422 nm.

The third-order optical nonlinearity, which is responsible for nonlinear refraction and nonlinear absorption of Ag NPs in aqueous solutions, is analyzed in Ref. [16]. They have shown the dependence of the nonlinear response on the nanoparticles' filling factor. The conventional Z-scan technique was employed, using 80 fs laser pulses at 800 nm, at the regimes of high and low pulse repetition rate. The thermo-optic nonlinear response of silver colloids containing Ag NPs of different sizes was reported in Ref. [17]. The colloidal nanoparticles were synthesized by laser ablation of bulk Ag in acetone using nanosecond pulses. The self-defocusing was the dominating process at the lowest power of laser radiation. Increase of concentration of nanoparticles in acetone led to increase of nonlinear refraction index, while the threshold power of OL was decreased. The thermal-induced self-defocusing and Kerr induced self-focusing in the Ag NP suspension prepared by laser ablation were investigated using femtosecond and nanosecond laser pulses at the wavelengths of 397.5, 532, and 795 nm [18]. The thermal-induced self-defocusing dominated at high pulse repetition rate as well as in the case of nanosecond probe pulses. In the case of low pulse repetition rate, the self-focusing and saturable absorption (SA) of picosecond and femtosecond pulses were observed in these colloidal solutions. The SA and reverse saturable absorption (RSA) influence the transient absorption spectroscopy of Ag NPs. These processes play important role while analyzing the properties of synthesized NPs in different spectral ranges [19].

Another nonlinear process which actively pursued using different NPs is the frequency conversion of strong laser field in the plasmas containing such species. The low-order nonlinearities of NPs, which are responsible for third harmonic generation in laser-produced plasmas (LPP), were studied in Ref. [20]. The LLPs are also considered as the attractive nonlinear media for conversion of the frequency of ultrashort infrared laser pulses towards the ultraviolet and extreme ultraviolet ranges [21, 22]. The advantages of using in situ produced Ag NPs for high-order harmonic generation (HHG) due to large nonlinear optical response of Ag NPs in the field of femtosecond probe pulses were analyzed in Ref. [23]. The spectral characteristics of harmonics from nanoparticles produced in situ were compared with the HHG from monoparticle plasma and with the HHG from preformed nanoparticle-containing plasma.

Meanwhile, to best of our knowledge, no systematic studies which combine the analysis of nonlinear absorption/refraction and lowest order harmonic generation in the same nanoparticle medium were reported so far. Each of abovementioned studies were focused on the particular properties of Ag NPs related with different components of their third-order nonlinear susceptibilities. Particularly, nobody analyzed in depth the correlation between different components of those susceptibilities. Here, we combine those groups of studies to demonstrate the fact that exceptionally strong nonlinearities (particularly, nonlinear absorption) out of the SPRs of nanoparticles strongly correlate with highly efficient third harmonic generation in Ag NPs. These studies show the way to explain the earlier reported exceptionally strong HHG conversion efficiency in Ag NP plasma by the specific properties of those particles related with involvement of

their plasmonic properties in the enhancement of nonlinear optical response in the extreme ultraviolet range.

In this paper, we present the results of systematic studies of the ablation-produced Ag NPs prepared by 5 ns, 200 ps, and 60 fs pulses at the wavelengths of 1064 and 800 nm. We demonstrate the OL in Ag NP suspension induced by two-photon absorption (2PA) and RSA at the wavelengths of 800 and 355 nm, respectively. We present the results of nonlinear refraction and nonlinear absorption studies using different wavelengths and pulse durations of laser radiation. Third harmonic generation (THG) in the plasmas containing Ag NPs is analyzed. We present the calculations of laser ablation of bulk Ag in liquid demonstrating NPs formation. We also discuss the advantages in application of small (8 nm) Ag NPs for low- and high-order harmonic generation of ultrashort laser pulses. Overall, we demonstrate the correlation between strong nonlinear optical response of silver nanoparticles out of their SPR and efficient THG in the plasmas containing Ag NPs.

2 Experimental arrangements for ablation and synthesis of Ag NPs in water and characterization of their nonlinear optical parameters

The Ag NPs were synthesized by ablation of bulk silver in water using nanosecond laser (Q-Smart 850, Coherent). Laser radiation (wavelength 1064 nm, pulse duration 5 ns, pulse repetition rate 10 Hz, pulse energy 40 mJ) was focused by 100 mm focal length lens on the surface of silver target immersed in deionized water (Fig. 1a). The target sizes were $5 \times 5 \times 2$ mm^3. The purity of our bulk silver target was 99.9%. The silver target was moved by two-coordinate translating stage during laser ablation. The ablation was carried out during 30 min. The color of suspension was changed during laser ablation until became yellow shade. We also ablated the silver target using 200 ps, 800 nm and 60 fs, 800 nm laser pulses. We did not observe any oxidation during and after laser ablation of pure silver target in deionized water. We also did not see any change of the color of our suspensions, which can indicate the change of SPR based on the change of the sizes of silver nanoparticles.

The nonlinear optical parameters of Ag NP suspension were investigated using Z-scan technique. We used different conditions for comparative analysis of the nonlinear optical parameters of suspensions. The nonlinear optical studies of Ag NP suspensions were carried out using nanosecond and femtosecond laser pulses at four different wavelengths (1064, 800, 400 and 355 nm). The closed-aperture (CA) and the open-aperture (OA) Z-scan schemes were used for nonlinear optical characterization of our samples. The radiation of Nd:YAG laser ($\lambda = 1064$ nm, $\tau = 5$ ns) or its third harmonic ($\lambda = 355$ nm) was focused by a 200 mm focal length lens (Fig. 1b). The beam waist diameters were 81 and 39 μm (at $1/e^2$ level of the spatial distribution at the focal plane) in the case of fundamental and third harmonic radiation, respectively. The energy of laser radiation was varied using neutral filters. The propagated pulses were detected by large aperture photodiode (DET100A/M, Thorlabs).

The 2-mm-thick fused silica cell containing Ag NP suspension was moved along the z-axis through the focal point using a translating stage. Attention was given to prevent the optical breakdown of studied medium. The intensities

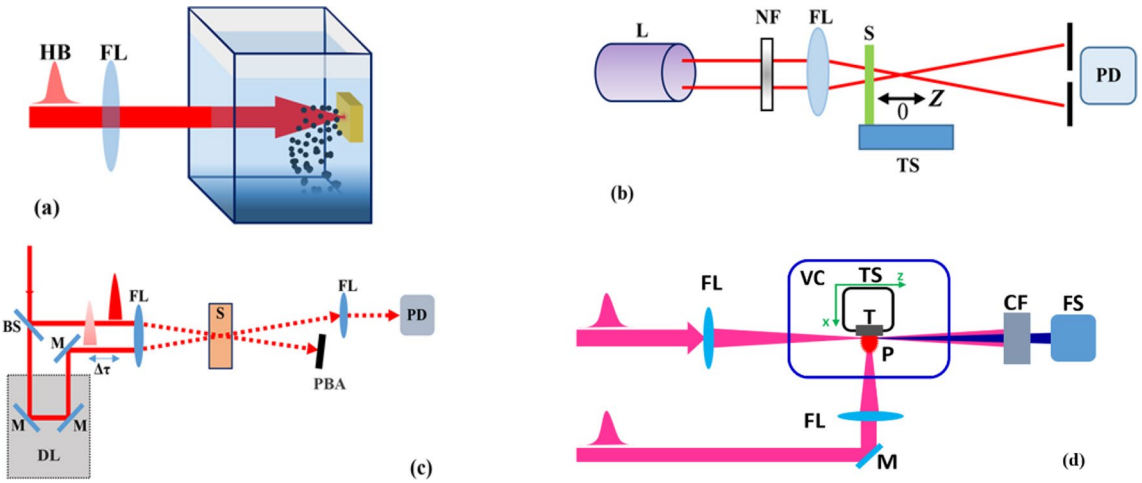

Fig. 1 **a** Experimental setup for laser ablation in liquid. *HB* heating beam, *FL* focusing lens. **b** Experimental setup for Z-scan studies. *L* Q-smart 850 nanosecond laser or Ti:sapphire femtosecond laser, *NF* neutral filters, *FL* focusing lens, *S* sample, *TS* translating stage, *PD* photodiode. **c** Experimental setup for pump–probe studies. *BS* beam splitter, *M* mirrors, *S* sample, *FL* focusing lenses, *PD* photodiode, *DL* delay line, *PBA* pump beam absorber. **d** Experimental scheme for third harmonic generation in laser plasma. *FL* focusing lenses, *M* mirror, *VC* vacuum chamber, *TS* translating stage, *T* target, *P* plasma, *CF* color filters, *FS* fiber spectrometer (USB2000)

of the optical breakdown of our suspensions in the case of nanosecond laser pulses were measured to be 6.4×10^9 and 1×10^9 W cm^{-2} at the wavelengths of fundamental and third harmonic radiation, respectively, while the maximal used intensities of probe radiation in the experiments did not exceed 1.6×10^9 ($\lambda=1064$ nm) and 6×10^8 W cm^{-2} ($\lambda=355$ nm). The Ti:sapphire laser (Spitfire Ace, Spectra Physics) provided 60 fs, 800 nm or 210 ps, 800 nm pulses at 1 kHz pulse repetition rate. The intensities of used femtosecond pulses ($\tau=60$ fs) did not exceed 2×10^{10} ($\lambda=800$ nm) and 1.6×10^{10} W cm^{-2} ($\lambda=400$ nm). The Z-scan scheme was calibrated using the known values of the nonlinear optical parameters of 1-mm-thick fused silica slides. The OL study was carried out by varying the energy of the pulses propagating through the quartz cell containing Ag NP suspension, which was installed in the focal plane. We did not add any surfactant to restrict the morphology variations of Ag NPs in water. The stability of morphology was controlled by analyzing the position of SPR during three months. We did not observe the notable change of SPR wavelength in the absorption spectra of our samples. Additionally, TEM and SEM studies confirmed the conclusion about good stability of synthesized NPs.

A noncollinear degenerate pump–probe technique was applied to study the transient absorption (TA) in Ag NPs. Laser radiation ($\lambda=400$ nm, $\tau=60$ fs) was split in two parts using beamsplitter. One part was used as a pump radiation and another part was used as a probe radiation, which was passed through the delay line to control the time separation between pump and probe pulses during their propagation through Ag NP suspension (Fig. 1c). Relative intensities and beam diameters of pump and probe pulses were adjusted to be approximately ~15:1 and 1:2. This study was performed at the wavelength of 400 nm obtained by doubling the frequency of fundamental radiation (800 nm) using barium borate (BBO) crystal. Pump pulse energy of 0.22 μJ was used for TA study.

In the case of THG studies the laser radiation ($\lambda=800$ nm, $\tau=60$ fs) was focused by a 400 mm focal length lens on the LPP (Fig. 1d). The beam waist radius of the focused radiation was 38 μm. The spectral characteristics of third harmonic radiation ($\lambda=266$ nm) were analyzed by a spectrometer (USB2000, Ocean Optics). To create plasma plume, a pulse was split from the Ti:sapphire laser by a beamsplitter before the compression of fundamental uncompressed pulse. The heating pulse duration was 210 ps. This radiation was focused on the target to heat it and produce LPP in the air conditions (Fig. 1d). The area of ablation was adjusted to be approximately 0.25 mm. A delay between fundamental and heating pulses was adjusted to be 38 ns. We also used different pressures of air by pumping vacuum chamber.

3 Results and discussion

3.1 Characterization of silver ablated in water and calculations of NPs formation using short laser pulses

TEM and SEM images and histograms of the Ag NPs prepared by ablation of bulk silver using pulses of different duration are presented in Fig. 2a–c. The linear absorption spectra of Ag NP suspensions (Fig. 2d) were measured using a spectrophotometer (Agilent Technologies). The SPRs of Ag NPs in two cases of ablation were observed at 402 nm. In the case of picosecond ablation the linear absorption coefficient of Ag NPs at $\lambda>450$ nm was larger compared to the case of nanosecond ablation. The sizes of NPs were measured to be 8 and 50 nm, by using the 5 ns and 210 ps pulses for laser ablation.

Below we present theoretical calculations of bulk silver ablation in water environment. Analysis of nanoparticle formation during laser ablation of metals is an excellent tool to estimate the precision of theoretical approaches for laser-matter interaction. However, for the best precision of computational approaches several factors have to be considered when determining the conditions of simulation. Characteristic feature of every bulk metal is the abundance of

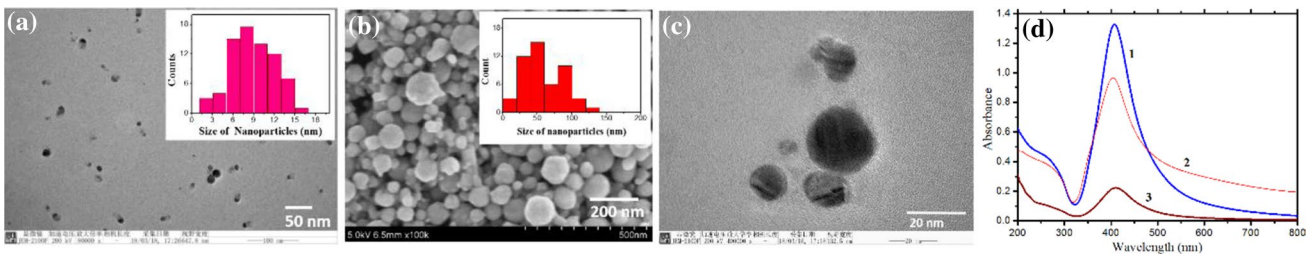

Fig. 2 **a** TEM image and histogram of size distribution of Ag NPs in the case of ablation in water using 1064 nm, 5 ns pulses, **b** SEM image and size distribution of Ag NPs ablated in water using 800 nm, 200 ps pulses, **c** TEM image of Ag NPs in the case of ablation in water using 800 nm, 60 fs pulses. **d** Absorption spectra of Ag NPs suspensions in case of ablation using (1) 1064 nm, 5 ns, (2) 800 nm, 200 ps and (3) 800 nm, 60 fs pulses

delocalized electrons. In metals the excess of free electrons leads to high plasma oscillation frequencies and extremely high reflection for IR and visible light. On the other hand, high concentration of free electrons means that the heat conductivity of metals is very high.

Optical penetration depth l_a is extremely small in metals due to negative refraction index, so in metals the total penetration depth

$$l = l_a + l_{th} \tag{1}$$

is actually the thermal penetration depth l_{th}, which is mostly determined by pulse duration:

$$l_{th} = 2\sqrt{K_e \tau_p}. \tag{2}$$

Here, K_e is heat conductivity due to electrons and τ_p is the pulse duration. Laser ablation of metals can be distinguished by pulse duration of the scale of femtoseconds, picoseconds and nanoseconds. As long as laser pulse duration exceeds electron–phonon relaxation time, the width of the heat-affected zone in metals can be estimated from Eq. (2). Shorter pulses reduce this zone and make the ablation process more uniform.

The process of laser ablation is split in two qualitatively different modes by intensity: below and above the plasma ignition threshold. A good estimate of the ablation regime is the Keldysh parameter:

$$\gamma = \sqrt{2\omega_0^2 I_p / E_0^2}. \tag{3}$$

Here, I_p is the ionization energy, ω_0 is the frequency of radiation and E_0 is the electric field strength. When $\gamma \ll 1$, the tunnel ionization is significant and the process is above the plasma ignition threshold. When $\gamma \gg 1$, the ablation is performed below the plasma ignition regime and the laser ablation can be separated from most the nonlinear optical processes. In our experiments the regime of ablation was below plasma ignition threshold. In this case, the analysis can be simplified by splitting the process in two parts: absorption of laser energy by free electrons and its further redistribution to atoms by electron–phonon coupling and to other electrons by electronic heat conductivity. The most general theoretical description of heat transfer during laser ablation can be performed within the so-called two-temperature model [24], which can be presented as:

$$C_i(T_i)\frac{\partial T_i}{\partial t} = \nabla[K_i \nabla T_i] - k(T_e - T_i) \tag{4}$$

$$C'_e(T_e)\frac{\partial T_e}{\partial t} = \nabla[K'_e \nabla T_e] - k(T_e - T_i) + S(x, y, z, t). \tag{5}$$

Here, subscript e denotes electrons, i denotes ions, K is heat conductivity, and k is the electron–phonon coupling constant. For our simulations of NPs formation we used molecular dynamical approach for the movement of atoms:

$$m_i \frac{d^2 \vec{r}_i}{dt^2} = -\sum_n \nabla U\left(\{\vec{r}_n\}\right)_i + \frac{k}{C_i}\frac{(T_e - T_i)}{T_i} m_i \frac{d\vec{r}_i}{dt}. \tag{6}$$

Here, m_i is the mass of ion (non-ionized atoms can be also considered here without loss of generality in case of metals), $\vec{r}_i$ is the position of ion, $U(\{\vec{r}_n\})_i$ is the pair interaction potential between the considered ion and the nth ion, and C_i is the heat capacity per one ion. The system of Eqs. (5) and (6) is approximately ten times more resource-demanding for numerical solution than solving Eqs. (5) and (6) separately or even solving the system (4) and (5). So it can be advantageous to solve the relations (4) and (5) first to get the heat flux transfer to ions and to solve single Eq. (6) for atoms with the corresponding velocity rescaling afterwards.

When the electron temperature (in units of energy) remains smaller than Fermi energy, the electron heat capacity and non-equilibrium electron thermal conductivity are given by [25]

$$C'_e = C_e(T_e)T_e \tag{7}$$

$$K_e = K_0(t)T_e/T. \tag{8}$$

Here, $K_0(t)$ is the conventional equilibrium thermal conductivity of metal and C'_e is a constant. Diffusion Eqs. (4) and (6) have three characteristic time scales: $\tau_e = C_e/k$, $\tau_i = C_i/k$ and τ_p which is the laser pulse duration. These three parameters define three distinctly different regimes of laser-metal interaction which are called femtosecond ($\tau_p \ll \tau_e$), picosecond ($\tau_i \gg \tau_p \gg \tau_e$) and nanosecond ($\tau_i \ll \tau_p$) regimes with regard to laser pulse duration. For investigation of dynamics of laser ablation at a picosecond time scale we used three-dimensional ITAP IMD molecular dynamics software [26] for simulation of laser ablation using 60 fs heating pulses in two-temperature mode (5–8). The calculation of molecular dynamics was continued for 80 ps after the application of the heating pulse because the transfer of the energy to atoms from electrons is not instantaneous. The laser was considered as a nearly-Gaussian pulse in time domain as:

$$S(x, y, z, t) = (1 - R)F(x, y)\alpha I(t)e^{-\alpha z}. \tag{9}$$

Here $F(x, y)$ is the Gaussian distribution in xy-plane, R is the reflectivity, $I(t)$ is intensity and α is the optical propagation constant for given frequency. We used the 95% reflectivity of silver when considering ablation by 800 nm radiation. The absorption coefficient for silver is given as $\alpha = 9 \times 10^7\ \mathrm{m}^{-1}$. For a Gaussian beam the lateral dimension of laser ablation is demonstrated to depend on the diameter d_f of laser beam on target surface and the threshold laser fluence for ablation F_0 at a given laser fluence $F(x, y)$:

$$d_{\mathrm{abl}} = d_{\mathrm{f}}\sqrt{\frac{1}{2}\ln\left(\frac{F(x,y)}{F_0}\right)}. \quad (10)$$

Hence, the ablation occurs primarily in the center of beam spot, while the edges of beam just heat up the target with the possible melting and evaporation on longer timescale. We consider the ablation in the center of spot with 100 μm radius irradiated by 0.5 mJ pulse with duration 60 fs. The dynamics of ablation is shown in Fig. 3 for the time intervals (a) 0, (b) 20, (c) 40, and (d) 80 ps from the beginning of ablation. It was observed that layers of thickness from 10 to 18 nm started to split from the sample after 40 ps of simulated time (Fig. 3c).

These results show reasonable coincidence with the experimental data on the sizes of nanoparticles. The calculation demonstrated that due to poor heat conductivity of deionized water the main role of surrounding medium during ablation is collecting of ablated nanoparticles. Thus this model could also be applied for analysis of plasma formation in vacuum when Ag NPs appear in the plasma plume during laser ablation.

3.2 Optical limiting in Ag NP suspension

Optical limiting is the important aspect for the application of nanostructured materials in nonlinear optics and laser physics particularly to protect sensitive systems and eyes from high-power laser radiation [27]. Earlier the optical limiting using Ag NPs was reported in Ref. [28]. It was shown that OL in these NPs in the field of nanosecond laser pulses at $\lambda = 532$ nm is much stronger than in other materials such as C_{60} and chloroaluminum phthalocyanine. Below we demonstrate the OL using 800 nm, 60 fs, and 355 nm, 5 ns laser pulses, which propagated through the suspension of Ag NPs in deionized water. The suspension was obtained during ablation of bulk silver using nanosecond laser pulses. This suspension was placed at the focal plane of 400 mm focal length lens.

The linear dependence between input and output 800 nm, 60 fs pulses was maintained up to the input pulse energy of ~0.6 μJ (Fig. 4a, filled triangles). Further growth of input pulse energy led to OL of propagated laser radiation due to 2PA. This process was maintained up to the energy of 800 nm pulses of ~2.0 μJ, which allowed stabilization of output energy at the level of 0.5 μJ along the 0.6–2.2 μJ energy range of input pulses. The OL in pure water was also studied in this energy range of propagated laser pulses. The slope of linear fitting for pure deionized water at small input pulse energies was equal to 1.0, while the slope of linear fitting of Ag NPs was equal to 0.7. The latter slope was corresponded to the initial transmittance of the suspension containing Ag NPs in deionized water. In the case of water we also observed the inclination of $I_{\mathrm{out}}/I_{\mathrm{in}}$ from the linear dependence due to white light generation (Fig. 4a, empty circles).

In the case of nanosecond laser pulses RSA led to the OL of 355 nm laser radiation. This process was analyzed in the range of energies between 150 and 600 μJ (Fig. 4b). One can see that Ag NP suspension demonstrated excellent OL properties in the case of nanosecond UV pulses. Our observations of the optical limiting in silver nanoparticles suspension were attributed to 2PA and RSA at the wavelengths of 800 nm and 355 nm probe pulses, respectively. During these experiments, the OL was analyzed by either increasing or decreasing the energy of laser pulses. In these two cases, we obtained the similarities with the same threshold energy for OL.

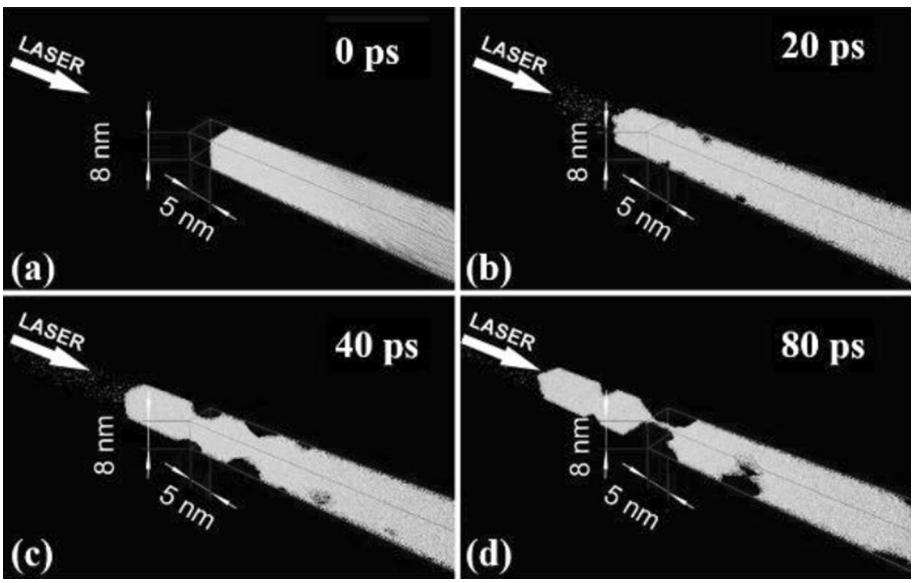

Fig. 3 Temporal evolution of laser plasma produced on the surface of bulk silver in the water environment at **a** 0, **b** 20, **c** 40, and **d** 80 ps from the beginning of irradiation by 60 fs pulses

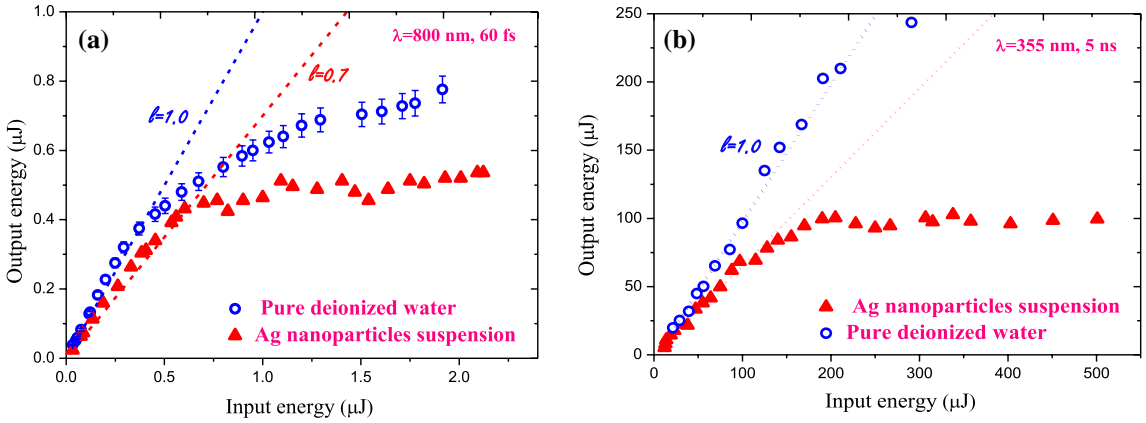

Fig. 4 Optical limiting in the aqueous suspension of Ag NPs (filled triangles) and pure water (empty circles) using **a** 60 fs, 800 nm, and **b** 5 ns, 355 nm probe pulses. Dotted lines show the linear dependences between output and input pulse energies at the lower energy ranges of input pulses

3.3 Nonlinear refraction and absorption in Ag NPs in the case of IR and UV laser pulses of different duration

The dependences of refractive indices and absorption coefficients of materials on the laser intensity are presented as [29]

$$n = n_0 + \gamma \times I \quad \text{and} \quad \alpha = \alpha_0 + \beta \times I. \tag{11}$$

Here, n_0 is the linear refractive index, I is the intensity of laser beam, γ and β are the nonlinear refractive index and nonlinear absorption coefficient of media, and α_0 is the linear absorption coefficient. The determination of γ and β of materials can be accomplished using the analysis of Z-scan curves. The Z-scan curves in the cases of CA and OA schemes for the bulk silver ablated in deionized water using nanosecond and picosecond pulses are shown in Fig. 5. Circles and squares represent the experimental data and solid lines are the theoretical fits. In case of CA Z-scan scheme the normalized transmittance [$T(z)$] is related to the nonlinear refractive index by

$$T(z) = 1 + 4\Delta\Phi_0 x/(x^2 + 1)(x^2 + 9). \tag{12}$$

Here, $x = z/z_0$, $z_0 = 0.5\ kw_o^2$ is the Rayleigh length, $k = 2\pi/\lambda$ is the wave number, w_o is the beam waist radius of the focused beam and $\Delta\Phi_0$ is the phase change. The nonlinear refractive index is related to the phase change as $\gamma = \Delta\Phi_0/kL_{\text{eff}}I_0$, where $L_{\text{eff}} = [1 - \exp(-\alpha_0 L)]/\alpha_0$ is the effective length of nonlinear medium, I_0 is the intensity of laser beam at the focal plane of focusing lens, and L is the sample thickness. The normalized transmittance curves were fitted with the CA experimental data. In the case of OA Z-scans, the photodetector measured the whole transmittance of propagated radiation. Figure 5a–d show the 2PA-induced OA Z-scans (empty circles). In that case the normalized transmittance of laser pulses can be described by

$$T(z) \approx 1 - q_0/2\sqrt{2}. \tag{13}$$

Here, $q_0(z) = I_0\beta L_{\text{eff}}/[1 + z^2/(z_0)^2]$. Equation (13) was fitted with the OA data presented in Fig. 5.

The nonlinear optical parameters were studied in the field of nanosecond and femtosecond laser pulses. The thermal induced self-defocusing was observed in the case of 1064 nm, 5 ns probe pulses (Fig. 5d, filled squares). The reverse process was observed in the case of 800 nm, 60 fs pulses at 1 kHz repetition rate (Fig. 5a–c, filled squares). This regime of interaction of femtosecond laser pulses with Ag NP suspension led to self-focusing, which is due to the electronic response of nanoparticles. The corresponding nonlin5ear optical parameters of 8 nm sizes Ag NPs in the case of 1064 nm, 5 ns probe laser pulses were: $\beta_{2PA} = 3.0 \times 10^{-10}$ cm W^{-1}, and $\gamma = -1.2 \times 10^{-14}$ cm^2 W^{-1}. At 800 nm, 60 fs probe pulses $\beta_{2PA} = 1.0 \times 10^{-10}$ cm W^{-1}, and $\gamma = 2.0 \times 10^{-15}$ cm^2 W^{-1}.

The Kerr-induced mechanism of self-defocusing for analysis of colloidal silver in the field of picosecond pulses has been considered in Ref. [30]. The thermal-induced effects can dominate over the fast Kerr-induced electronic contribution when the probe pulse duration becomes longer than the thermal conductivity relaxation time of small sized Ag NPs. Hence, the duration of laser pulses is a critical parameter for the evaluation of third-order nonlinear response, especially nonlinear refraction.

The dependences of OA and CA normalized transmittances of Ag NP suspensions at the wavelength of 400 nm femtosecond laser pulses are shown in Fig. 6. The 2PA, SA, and RSA parameters of used suspension at this

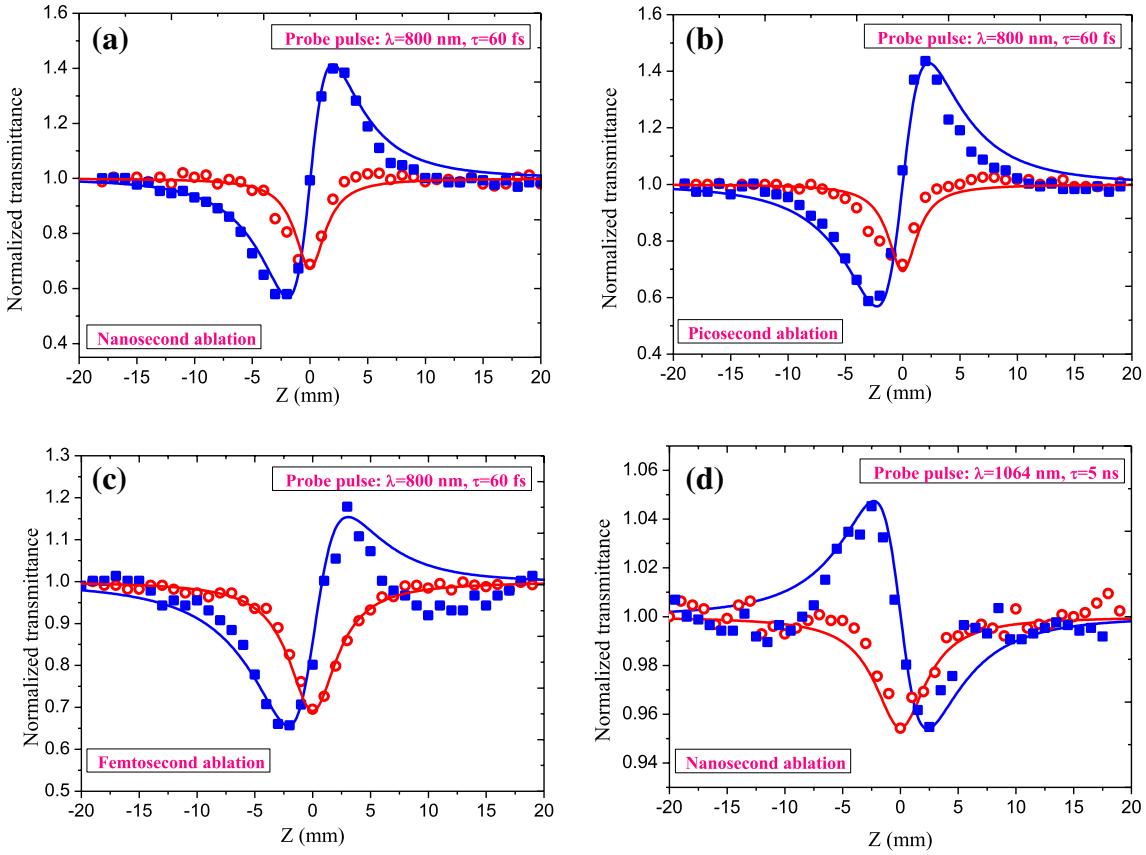

Fig. 5 OA and CA Z-scans of Ag NP suspensions prepared by laser ablation of solid target using **a** 5 ns, 1064 nm, **b** 200 ps, 800 nm, and **c** 60 fs, 800 nm laser pulses. 60 fs, 800 nm pulses were used as a probe radiation in the **a**–**c** cases. **d** OA and CA curves in the case of 5 ns, 1064 nm probe pulses. Ag NPs were prepared using 5 ns, 1064 nm pulses. Solid curves are the fits to experimental data (see text)

wavelength were calculated by fitting the experimental data with the Eq. (13) and the relation describing SA:

$$T_{\mathrm{SA}}(z) = 1 + \frac{I_{\mathrm{o}}}{I_{\mathrm{sat}}(x^2+1)}, \tag{14}$$

where I_{sat} is the saturated intensity of the medium.

Figure 6a demonstrates three processes: SA, RSA and self-focusing in silver nanoparticles suspension at 400 nm, 60 fs probe pulses. Our studies showed the dominance of the self-focusing process at higher energies of probe pulses. We fitted these data using the equation for three processes: SA, RSA and self-focusing.

The results of similar OA studies of Ag NP suspension ablated by nanosecond radiation using 355 nm, 5 ns probe pulses are shown in Fig. 7a. The corresponding nonlinear absorption coefficients of the studied samples at $\lambda = 355$ nm were as: $\beta_{\mathrm{SA}} = -3\times10^{-11}$ cm W^{-1}, and $\beta_{\mathrm{RSA}} = 2\times10^{-10}$ cm W^{-1}.

Figure 7b shows self-defocusing and 2PA of 355 nm laser radiation in Ag NP suspension ablated by picosecond laser pulses. The nonlinear optical parameters of the Ag NP suspensions measured at different experimental conditions are collected in Table 1. Notice that the concentration of Ag NPs in the case of femtosecond ablation was notably smaller than concentration of the NPs produced during ablation using picosecond and nanosecond pulses due to less efficient ablation in the former case. Because of this, the nonlinear optical response of these species under the action of nanosecond probe pulses was at the threshold of registration.

Notice that actual values of the nonlinear susceptibilities of NPs are considerably larger than those of NP suspensions due to small fraction of nanoparticles in the whole volume of solvent. A simple and well-established method for estimation of the nonlinear susceptibilities of nanoparticles is to divide the nonlinear susceptibility of compound by the volume or weight part of NPs. In fact, the third-order nonlinear susceptibilities $[\chi^{(3)}]$ of composites, and correspondingly, γ and β, are also depend on the local field factor as

$$\chi^{(3)} = p|f|^2 f^2 \chi^{(3)}_{\mathrm{NPs}}. \tag{15}$$

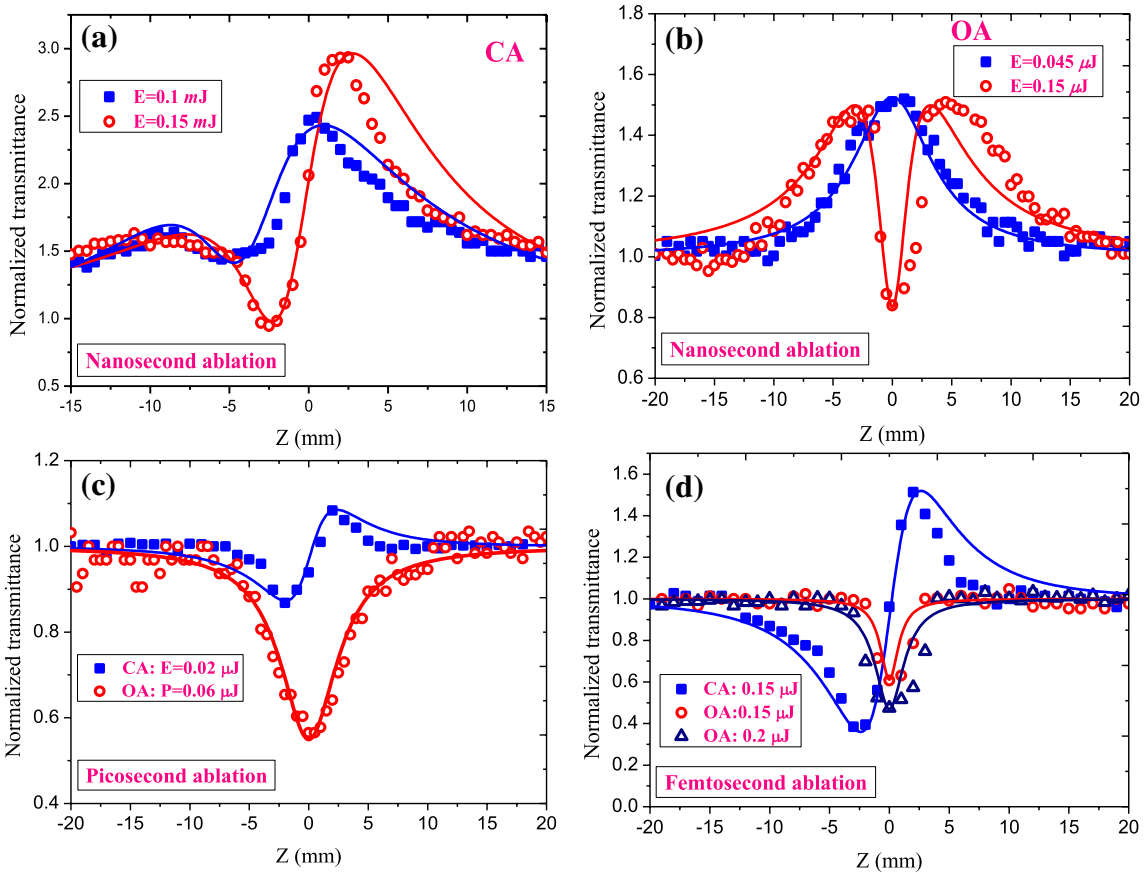

Fig. 6 Measurements using 400 nm, 60 fs pulses. **a** CA, and **b** OA Z-scans of Ag NP suspension produced by 5 ns, 1064 nm pulses at different energies of probe pulses. **c** OA and CA Z-scans of Ag NP suspension produced by 200 ps, 800 nm pulses. **d** OA and CA Z-scans of Ag NP suspension produced by 60 fs, 800 nm pulses

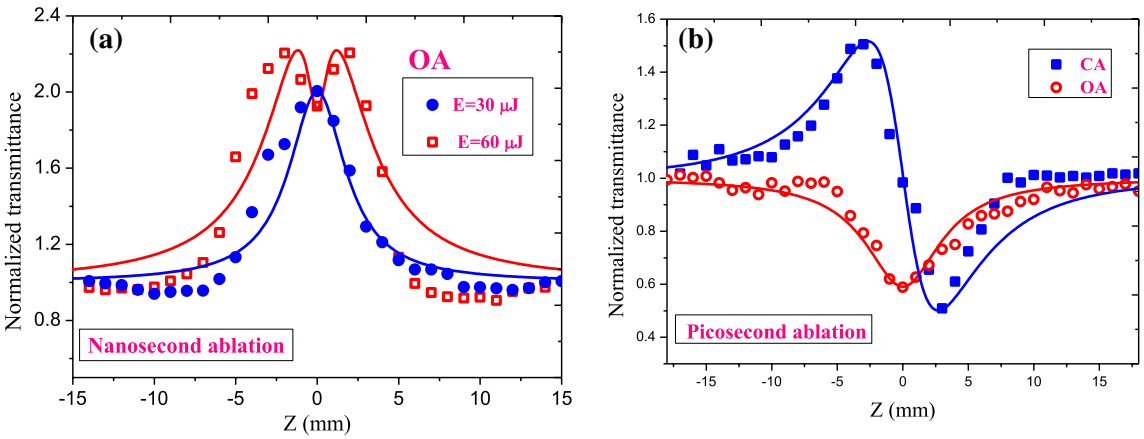

Fig. 7 **a** SA and RSA in Ag NP suspensions prepared by ablation using nanosecond pulses at different energies of 355 nm, 5 ns probe pulses: (filled circles) 30 μJ, and (empty squares) 60 μJ. **b** Self-defocusing and 2PA using 355 nm, 5 ns laser pulses ($E=50$ μJ) in the case of the suspension prepared by picosecond pulses

Here, $\chi^{(3)}_{\mathrm{NPs}}$ is the third-order nonlinear susceptibility of NPs, f is the local field factor, and p is the filling factor (i.e., volume or weight part). The enhancement due to local field factor is insignificant in the case of metal NPs far from their SPRs. In particular, the insignificant enhancement of local

Table 1 Nonlinear optical parameters of Ag NP suspensions

		Ag NPs (8 nm)	Ag NPs (50 nm)	Ag NPs (15 nm)
		Parameters of heating pulses		
		$\lambda = 1064$ nm, $\tau = 5$ ns, $E = 40$ mJ	$\lambda = 800$ nm, $\tau = 200$ ps, $E = 0.56$ μJ	$\lambda = 800$ nm, $\tau = 60$ fs, $P = 0.96$ μJ
800 nm, 60 fs	γ (cm^2 W^{-1})	2.0×10^{-15}	3.4×10^{-15}	1.9×10^{-15}
	β_{2PA} (cm W^{-1})	1.0×10^{-10}	0.9×10^{-10}	0.9×10^{-10}
	$\chi^{(3)}$ (esu units)	1.8×10^{-9}	2.6×10^{-9}	1.6×10^{-9}
400 nm, 60 fs	γ (cm^2 W^{-1})	2.1×10^{-15}	1.5×10^{-15}	3.2×10^{-15}
	β (cm W^{-1})	RSA: 8.6×10^{-10}	RSA: 5.5×10^{-10}	2PA: 5.5×10^{-10}
	β_{SA} (cm W^{-1})	-1.9×10^{-10}	–	–
	$\chi^{(3)}$ (esu units)	3.6×10^{-9}	2.8×10^{-9}	3.3×10^{-9}
1064 nm, 5 ns	γ (cm^2 W^{-1})	-1.2×10^{-14}	–	–
	β_{2PA} (cm W^{-1})	3.0×10^{-10}	–	–
	$\chi^{(3)}$ (esu units)	0.6×10^{-9}	–	–
355 nm, 5 ns	γ (cm^2 W^{-1})	–	-2.5×10^{-15}	–
	β_{RSA} (cm W^{-1})	2.0×10^{-10}	9.0×10^{-10}	–
	β_{SA} (cm W^{-1})	-3.0×10^{-11}	–	–
	$\chi^{(3)}$ (esu units)	-0.2×10^{-9}	0.8×10^{-9}	–

field factor for Mn nanoparticles suspension was reported in Ref. [31]. In the case of Ag NPs $|f|^2$ is in the range of 0.1 and 1 in non-resonance conditions (i.e. at the wavelengths of 800, 1064, and 355 nm). In the resonance conditions, the local field factor increases become equal to 3.6 at 400 nm. The f of small-sized Ag NPs at different wavelengths was estimated in Ref. [32] where the influence of the local field factor on the power of probe pulse, particle size and photon energy around the SPR was analyzed. The role of the SPR of Ag NPs was also studied in Refs. [18, 33].

Third-order nonlinear susceptibilities in media having nonlinear absorption and refractive index can be considered to be a complex quantity

$$\chi^{(3)} = \mathrm{Re}\,\chi^{(3)} + i\,\mathrm{Im}\,\chi^{(3)} \tag{16}$$

where, the imaginary part is related to the nonlinear absorption coefficient through

$$\mathrm{Im}\,\chi^{(3)} = \frac{n^2\varepsilon_0 c\lambda\beta}{2\pi} \tag{17}$$

and the real part is related to γ through

$$\mathrm{Re}\,\chi^{(3)} = 2n^2\varepsilon_0 c\gamma. \tag{18}$$

Here, ε_0 is the permittivity of free space. For the presentation of $\chi^{(3)}$ in esu units, we used the relation $\chi^{(3)}$ [esu units] $= (9\times10^8/4\pi)\chi^{(3)}$ [SI units]. We calculated $\chi^{(3)}$ of NP suspensions and included these results in Table 1.

In Ref. [34], the nonlinear refraction index in larger sized nanoparticles is higher than in small NPs. The authors of this paper have also shown that the nonlinear refractive index larger for 17 nm Ag NPs with regard to 13 nm Ag NPs. Switching from SA at lower intensities to RSA at higher intensities is explained through the transitions of conduction band electrons to higher excited states. In our case, we obtained the switching of SA to RSA and self-focusing at highest used intensities of 400 nm, 60 fs laser pulses.

The parameters shown in Table 1 are attributed to the suspensions of Ag NPs. Our estimates show that the volume fraction of NPs in suspensions was in the range of 10^{-3}. The values of γ and β of Ag NPs with 8 nm sizes can be multiplied by a factor of 1.0×10^5 for 1064 nm (i.e. far from SPR) and 11.0 for 400 nm pulses (i.e. in the resonance conditions) to determine these parameters attributed to Ag NPs taking into account the f defined from Ref. [32]. In particular, β of suspension measured by 1064 nm, 5 ns and 400 nm, 60 fs probe pulses was measured to be 3.0×10^{-10} cm W^{-1}, and 8.6×10^{-10} cm W^{-1}. One can estimate β of NPs at these conditions to be 3.0×10^{-5} cm W^{-1}, and 9.4×10^{-9} cm W^{-1} respectively.

During these studies the 2PA cross section of Ag NPs was calculated. We used the β_{2PA} values of Ag NPs for determination of the 2PA cross section (σ_{2PA}) using the following relation

$$\sigma_{2PA} = (10^3 \times h\nu \times \beta_{2PA})/N_A V \tag{19}$$

where h is Planck's constant, ν is the frequency of light, N_A is the Avogadro's number, and V is the volume fraction of nanoparticles. The value of the 2PA cross section for the 2PA absorption coefficient of the Ag NPs at 800 nm, 60 fs probe pulses was calculated to be 3.6×10^{-47} cm^4 s photon^{-1}.

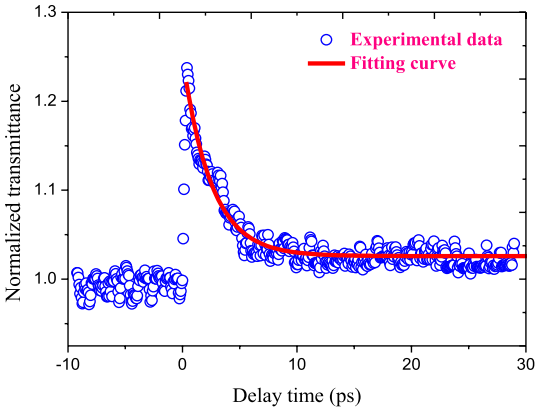

Fig. 8 Pump–probe measurements of Ag NP suspension at the wavelength of 400 nm using 60 fs laser pulses

3.4 Transient absorption measurements

Figure 8 shows the pump–probe data for 8 nm Ag NPs prepared by ablation using nanosecond pulses in deionized water. The TA curve for Ag NPs in water was fitted with single exponential fit (solid curve). The profile of pump–probe signal of Ag NPs in deionized water indicates the process of photo-bleaching due to the resonant excitation at 400 nm (see also Fig. 6b, filled squares). The lifetime of excited plasmon for Ag NPs at 400 nm was measured to be 2.5 ps, which can be assigned to the electron–phonon relaxation time. In the case of 50 nm Ag NPs we did not observe similar temporal response at the wavelength of 400 nm. This behavior could be explained by the size dependence and the nonlinear optical response of electron–phonon interaction dynamics of the Ag NPs. The theoretical approaches for calculating the ultrafast nonlinear optical responses of dielectric composite materials consisting of metal nanoparticles with different sizes and shapes are described in Refs. [35, 36]. The nonlinear local field effect in Ag nanoparticles was also studied in Ref. [31]. For particles with smaller sizes the relaxation process due to electron–phonon interaction is faster than for particles with larger sizes. It was shown that red shift of the peaks of the SPR related to increase of Ag NPs sizes led to the change of the nonlinear absorption in the field of femtosecond laser pulses.

For understanding the dynamics of electron relaxation in excited Ag NPs at resonance conditions we used the Z-scan and pump–probe data. One can determine the cross-section of bleaching of the Ag NPs by equation [37]:

$$s_{12} = h\nu/(2I_{\text{sat}} \times t_{21}) \quad (20)$$

where σ_{12} is the absorption cross section of Ag NPs and τ_{21} is the relaxation time of electron–phonon interaction. Using this equation and values of saturation intensities $I_{\text{sat}} = 6.3 \times 10^8$ W cm^{-2} at 355 nm, 5 ns and $I_{\text{sat}} = 2.4 \times 10^{10}$ W cm^{-2} at 400 nm, 60 fs probe pulses we calculated the excited state absorption cross sections at the wavelengths of 355 nm and 400 nm as 6.7×10^{-16} and 8×10^{-17} cm^2 respectively.

3.5 Third harmonic generation in laser-produced plasmas containing Ag NPs

Prior to the THG studies, we analyzed the structural and optical properties of deposited thin films on the surfaces of quartz and silicon substrates to proof the presence of Ag NPs during ablation of silver target in air. The absorption spectrum of the deposited thin films showed the appearance of SPR at 415 nm due to the formation of Ag NPs (Fig. 9). The atomic force microscopy (AFM) of the deposited silver films showed broad distribution of NPs' sizes. Our theoretical analysis also showed that small sized Ag NPs started to evaporate 80 ps from the beginning of irradiating the bulk silver target using 200 ps, 800 nm pulses. Formation of NPs during ablation of thin films has also been predicted in Ref. [38].This type of ablation facilitates condensation of metal atoms into clusters and rapid growth of the atomic clusters into nanoparticles with maximum sizes barely exceeding 10 nm. The NPs with large sizes at around 100 nm did not contribute to low-order harmonic process. The velocity of nanoparticles depend on the mass and fluence of heating beam [39]. Only small clusters appear in the area of interaction at the moment of femtosecond pulse arrival (i.e. 38 ns from the beginning of ablation). Thus these species are responsible for harmonic generation in present conditions.

We analyzed the advantages in application of small Ag NPs for low-order harmonic generation of femtosecond laser pulses. Some previous studies using the atomic plasmas produced on the surfaces of bulk silver target and the

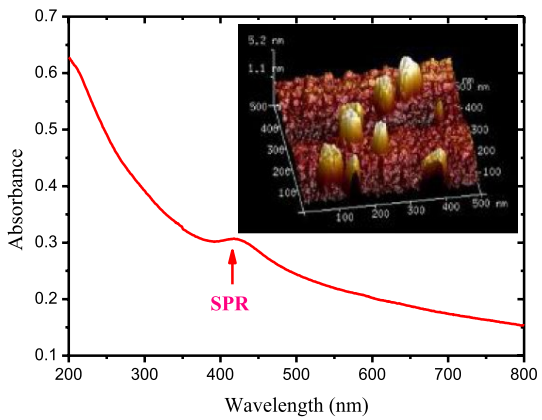

Fig. 9 Absorption spectra of the deposited silver on the surface of quartz substrate using 800 nm, 200 ps heating laser pulses. Inset: AFM of deposited films showing presence of Ag NPs on the deposited surfaces of quartz substrate

plasmas containing Ag NPs have shown relatively high conversion efficiency of harmonics generated in such media [40]. The usefulness in application Ag NPs for enhancement of HHG in the extreme ultraviolet range has also been demonstrated in Ref. [41].

Figure 10 presents the spectra and the intensity of the third harmonic (TH) as a function of the probe and the heating pulse intensity in the plasma plumes containing Ag NPs. One can see a sixfold enhancement of TH efficiency in the case of air conditions compared with the THG in air. We also analyzed relation TH yield at the air pressure of 1.3 kPa. In this case, we obtained the 20× enhancement of TH yield from Ag plasma with regard to residual air. A slope of fitting line in Fig. 10b corresponds to 3, which is the indication of the expected cubic dependence between fundamental and harmonic pulses in the case of THG. Figure 10c shows the dependence of TH yield on the heating pulse energy. We did not observe saturation of THG at the highest used energy of heating picosecond pulses (0.5 mJ).

Figure 11a shows the dependence of the TH yield at different angles of rotation of quarter-wave plate, which caused variation of the polarization of driving radiation from linear (at 0°) to circular (at 45°). A deviation from linear polarization led to a decrease of TH intensity, which is typical for low- and high-order harmonics. The application of circularly polarized laser pulses led to complete disappearance of harmonic emission, as it should occur assuming the origin of the harmonic generation process.

Figure 11b shows the Z-scan of THG performed for Ag plasma by changing position of focusing lens of the probe pulses. These measurements were carried out at 1.2×10^{11} W cm^{-2} intensity of probe pulses in the focal plane. Further increase of intensity of femtosecond pulses in the focal position led to the decrease of THG at $z=0$ position of plasma plumes. This behavior can be explained by

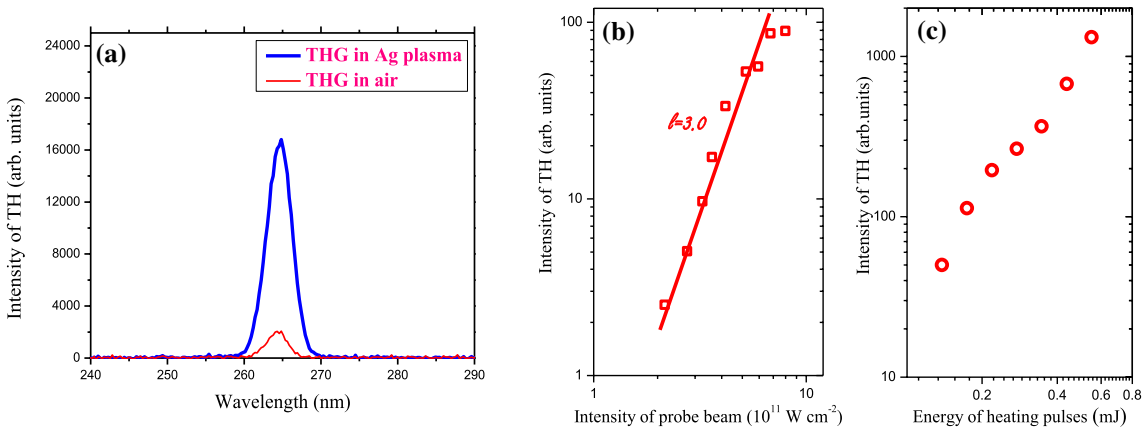

Fig. 10 **a** Spectra of the third harmonic generation in the plasma containing Ag NPs (thick curve) and in the air (thin curve). **b** Dependence of the intensity of TH on the intensity of femtosecond laser pulses in silver plasma. **c** Dependence of the intensity of TH on the energy of heating picosecond laser pulses

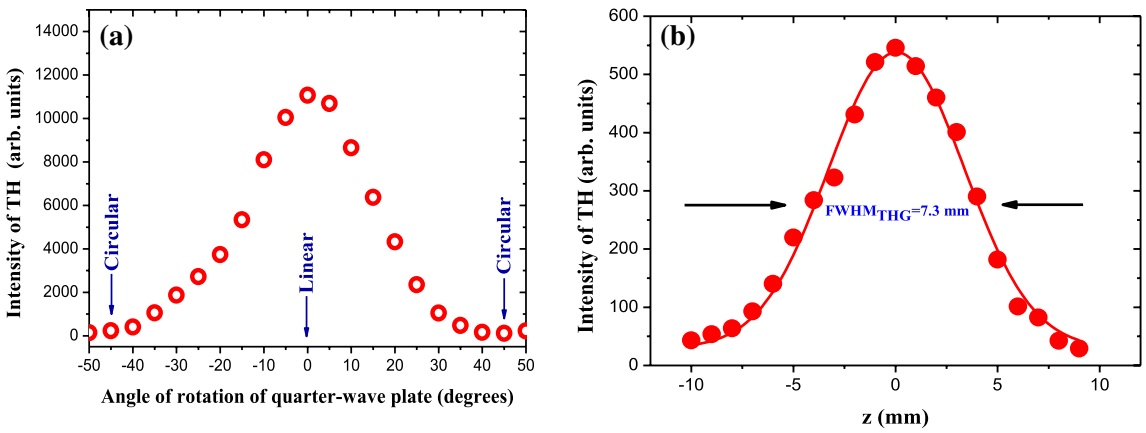

Fig. 11 **a** Dependence of TH intensity on the angle of rotation of the quarter-wave plate. **b** Dependence of THG on the position of plasma plume with regard to the focal plane of probe pulses. The intensity of laser beam in the focal plane was 1.2×10^{11} W cm^{-2}

phase mismatch of interacting waves due to the growth of concentration of the electrons in the interaction zones. The theoretical model for the calculation of electron concentration at these conditions was developed in Ref. [42]. This model can be applied to a wide range of plasma conditions.

The conversion towards 266 nm radiation in the case of plasma plume was notably stronger compared with THG in air. We defined the THG conversion efficiencies in air and Ag NP plasmas to be 1×10^{-3} and 4×10^{-3} in the case of 800 nm, 60 fs driving pulses. The value of conversion efficiency in air was comparable with earlier reported studies carried out at similar conditions [43, 44]. We attribute the TH enhancement to the involvement of small silver clusters in the harmonic generation.

4 Conclusions

We have analyzed the Ag NPs prepared during ablation of bulk silver in deionized water using different wavelengths and durations of heating pulses. Their structural, optical and low-order nonlinear optical parameters were determined. The joint appearance of nonlinear optical refraction and absorption was analyzed using the 1064 nm, 5 ns and 800 nm, 60 fs probe pulses. The study of the nonlinear optical parameters of Ag NPs in the resonant and quasi-resonant conditions using 400 nm, 60 fs pulses have shown the presence of SA and RSA. The nonlinear absorption coefficient of suspensions was as high as 3.0×10^{-5} cm W^{-1} at the wavelength of 1064 nm. The Ag NP suspension has demonstrated the outstanding optical limiting properties in the case of 355 nm, 5 ns probe pulses. Nonlinear refraction showed the change of sign with variation of the wavelength and duration of laser pulses.

The nonlinear optical properties of small-sized nanoparticles are related with the quantum confinement effect. Particularly, in the case of semiconductor nanoparticles, one has to take into account the variation of the band gap with the change of nanoparticles sizes. In our case, we observed the increase of the nonlinear refractive index for 50 nm Ag NPs with regard to smaller sized NPs using 800 nm, probe pulses. Meanwhile, in the case of 400 nm probe pulses the reverse case was observed.

The lifetime of excited plasmon for Ag NPs at 400 nm was measured to be 2.5 ps, which can be assigned to the electron–phonon relaxation time. The excited state absorption cross sections of Ag NPs at different wavelengths were determined. We also presented the theoretical studies of the laser ablation of silver in water. The application of small-sized nanoparticles for low-order harmonic generation of femtosecond laser pulses was demonstrated and systematically analyzed during ablation of silver in air. The enhancement of low-order harmonic generation is attributed to the influence of silver clusters on the nonlinear optical response of Ag plasma. These studies, for the first time, have demonstrated the involvement of multi-atomic Ag particles in the growth of third harmonic yield. The conversion towards 266 nm radiation in the case of plasma plume was notably stronger compared with THG in air. We defined the THG conversion efficiencies in air and Ag NP plasmas to be 1×10^{-3} and 4×10^{-3} in the case of 800 nm, 60 fs driving pulses.

The selection of the topics of these studies follows with some logical sequences. OL effect is a process caused by the nonlinear optical properties of materials. It can be explained by Z-scan data. We also analyzed the cross section of excited states using the saturable absorption data and transient absorption profile. Finally, we demonstrated, through harmonic generation, that ablation and formation of nanoparticles in liquid and air has the advantages, which can be used for high-order harmonic generation in the laser-produced silver plasmas containing nanoparticles and quantum dots. Furthermore, the increase of third harmonic yield in the plasmas containing silver nanoparticles allows basic explanation of the formation silver nanoparticles at different conditions.

In conclusion, we have presented two groups of studies to demonstrate the fact that exceptionally strong nonlinearities (particularly, nonlinear absorption) strongly correlate with highly efficient third harmonic generation in Ag NPs. Particularly, we have shown the correlation between strong nonlinear optical response of silver nanoparticles in IR range and efficient third-order harmonic generation in the plasmas containing Ag NPs. These studies show the way to attribute the earlier reported exceptionally strong HHG conversion efficiency in Ag NP plasma to the specific features of those particles related with involvement of their plasmonic properties in the enhancement of nonlinear optical response in the extreme ultraviolet range.

Acknowledgements RAG thanks the financial support from Chinese Academy of Sciences President's International Fellowship Initiative (Grant no. 2018VSA0001).

Funding Natural Science Foundation of China (61774155, 61705227), National Key Research and Development Program of China (2017YFB1104700).

References

1. T. Jia, M. Baba, M. Suzuki, R.A. Ganeev, H. Kuroda, J. Qiu, X. Wang, R. Li, Z. Xu, Fabrication of two-dimensional periodic nanostructures by two-beam interference of femtosecond pulses. Opt. Express **16**, 1874 (2008)
2. L. Jiang, A. Wang, B. Li, T. Cui, Y. Lu, Electrons dynamics control by shaping femtosecond laser pulses in micro/nanofabrication:

modeling, method, measurement and application. Light Sci. Appl. **7**, 17134 (2018)
3. R.A. Ganeev, M. Suzuki, M. Baba, M. Ichihara, H. Kuroda, Low- and high-order nonlinear optical properties of $BaTiO_3$ and $SrTiO_3$ nanoparticles. J. Opt. Soc. Am. B **25**, 325 (2008)
4. E.V. Garcia Ramirez, S.A. Sabinas Hernandes, D. Ramires Martines, G. Diaz, J.A. Reyes, Esqueda, Third order nonlinear optics in Ag nanocubes: local and nonlocal optical responses as a function of excitation wavelength and particles. Opt. Express **25**, 31064 (2017)
5. S. Porel, N. Venkatram, D. Narayana Rao, T.P. Radhakrishnan, Optical power limiting in the femtosecond regime by silver nanoparticle–embedded polymer film. J. Appl. Phys. **102**, 033107 (2007)
6. O. Muller, S. Dengler, G. Ritt, B. Eberle, Size and shape effects on the nonlinear optical behavior of silver nanoparticles for power limiters. Appl. Opt. **52**, 139 (2013)
7. R.A. Ganeev, M. Baba, A.I. Ryasnyansky, M. Suzuki, H. Kuroda, Laser ablation of GaAs in liquids: structural, optical, and nonlinear optical characteristics of colloidal solutions. Appl. Phys. B **80**, 595 (2005)
8. C.H. Bae, S.H. Nam, S.M. Park, Formation of Ag NPs by laser ablation of a silver target in NaCl solution. Appl. Sur. Sci. **197–198**, 628 (2002)
9. M. Procházka, J. Štěpánek, B. Vlčková, I. Srnová, P. Malý, Laser ablation: preparation of "chemically pure" Ag colloids for surface-enhanced Raman scattering spectroscopy. J. Mol. Struct. **410–411**, 213 (1997)
10. K.G. Stamplecoskie, J.C. Scaiano, V.S. Tiwari, H. Anis, Optimal size of silver nanoparticles for surface-enhanced Raman spectroscopy. J. Phys. Chem. C **115**, 1403 (2011)
11. M. Darroudi, M. Ahmad, R. Zamiri, R. Abdullah, A. Ibrahim, N. Shameli, K. Shahril, M. Husin, Preparation and characterization of gelatin mediated Ag NPs by laser ablation. J. Alloys Compd. **509**, 1301 (2011)
12. M. Valverde-Alva, T. García-Fernández, M. Villagrán-Muniz, C. Sánchez-Aké, R. Castañeda-Guzmán. E. Esparza-Alegría. C. Sánchez-Valdés. J. Llamazares, C. Herrera, Synthesis of Ag NPs by laser ablation in ethanol: a pulsed photoacoustic study. Appl. Surf. Sci. **355**, 341 (2015)
13. V. Nikolov, R. Nikov, I. Dimitrov, N. Nedyalkov, P. Atanasov, M. Alexandrov, D. Karashanova, Modification of the Ag NPs size-distribution by means of laser light irradiation of their water suspensions. Appl. Surf. Sci. **280**, 55 (2013)
14. M. Darroudi, M. Ahmad, R. Zamiri, A. Abdullah, N. Ibrahim, A. Sadrolhosseini, Time-dependent preparation of gelatin-stabilized Ag NPs by pulsed Nd:YAG laser. Solid Stat. Sci. **13**, 520 (2011)
15. R. Das, S. Nath, D. Chakdar, G. Gope, R. Bhattacharjee, Synthesis of Ag NPs and their optical properties. J. Exp. Nanosci. **5**, 357 (2010)
16. D. Rativa, R.E. De Araujo, A.S.L. Gomes, One photon nonresonant high-order nonlinear optical properties of Ag NPs in aqueous solution. Opt. Express **16**, 19244 (2008)
17. M. Mashayekh, D. Dorranian, Size-dependent nonlinear optical properties and thermal lens in Ag NPs. Optik **125**, 5612 (2014)
18. R.A. Ganeev, M. Baba, A.I. Ryasnyansky, M. Suzuki, H. Kuroda, Characterization of optical and nonlinear optical properties of Ag NPs prepared by laser ablation in various liquids. Opt. Commun. **240**, 437 (2004)
19. R.A. Ganeev, A.I. Ryasnyansky, A.L. Stepanov, T. Usmanov, Saturated absorption and reverse saturated absorption of $Cu:SuO_2$ at $\lambda = 532$ nm. Phys. Status Solidi B **241**, R1 (2004)
20. M. López-Arias, M. Oujja, M. Sanz, R.A. Ganeev, G.S. Boltaev, N.K. Satlikov, R.I. Tugushev, T. Usmanov, M. Castillejo, Low-order harmonic generation in metal ablation plasmas in nanosecond and picosecond regimes. J. Appl. Phys. **111**, 043111 (2012)
21. R.A. Ganeev, M. Suzuki, M. Baba, H. Kuroda, High harmonic generation from the laser plasma produced by the pulses of different duration. Phys. Rev. A **76**, 023805 (2007)
22. T. Ozaki, L.B. Elouga Bom, R. Ganeev, J.-C. Kieffer, M. Suzuki, H. Kuroda, Intense harmonic generation from silver ablation. Laser Part. Beams **25**, 321 (2007)
23. H. Singhal, R.A. Ganeev, P.A. Naik, J.A. Chakera, U. Chakravarty, H.S. Vora, A.K. Srivastava, C. Mukherjee, C.P. Navathe, S.K. Deb, P.D. Gupta, High-order harmonic generation in a plasma plume of *in situ* laser-produced silver nanoparticles. Phys. Rev. A **82**, 043821 (2010)
24. D.S. Ivanov, L.V. Zhigilei, Combined atomistic-continuum modeling of short-pulse laser melting and disintegration of metal films. Phys. Rev. B **68**, 064114 (2003)
25. B.N. Chichkov, C. Momma, S. Nolte, F. von Alvensleben, A. Tünnermann, Femtosecond, picosecond and nanosecond laser ablation of solids. Appl. Phys. A **63**, 109 (1996)
26. J. Stadler, R. Mikulla, H.-R. Trebin, IMD: a software package for molecular dynamics studies on parallel computers. Int. J. Mod. Phys. C **8**, 1131 (1997)
27. R.A. Ganeev, Nonlinear refraction and nonlinear absorption of various media. J. Opt. A **7**, 717 (2005)
28. Y.-P. Sun, J.E. Riggs, H.W. Rollins, R. Guduru, Strong optical limiting of silver-containing nanocrystalline particles in stable suspension. J. Phys. Chem. B **103**, 77 (1999)
29. N. Faraji, W.M.M. Yunus, A. Kharazmi, E. Saion, M. Shahmiri, N. Tamchek, Synthesis, characterization and nonlinear optical properties of silver/PVA nanocomposites. J. Eur. Opt. Soc. Rapid Publ. **7**, 12040 (2012)
30. R.A. Ganeev, A.I. Ryasnyansky, S.R. Kamalov, M.K. Kodirov, T. Usmanov, Nonlinear susceptibilities, absorption coefficients and refractive indices of colloidal metals. J. Phys. D Appl. Phys. **34**, 1602 (2001)
31. R.A. Ganeev, A.S. Zakirov, G.S. Boltaev, R.I. Tugushev, T. Usmanov, P.K. Khabibullaev, T.W. Kang, A.A. Saidov, Structural, optical, and nonlinear optical absorption/refraction studies of the manganese nanoparticles prepared by laser ablation in ethanol. Opt. Mater. **33**, 419 (2011)
32. R. Sato, M. Ohnuma, K. Oyoshi, Y. Takeda, Spectral investigation of nonlinear local field effects in Ag nanoparticles. J. Appl. Phys. **117**, 113101 (2015)
33. R.A. Ganeev, A.I. Ryasnyansky, A.L. Stepanov, T. Usmanov, Characterization of nonlinear-optical parameters of copper- and silver-doped silica glass. Phys. Status Solidi B **241**, 935 (2004)
34. G.K. Podagatlapalli, S. Hamad, S.P. Tewari, S. Sreedhar, M.D. Prasad, S.V. Rao, Silver nano-entities through ultrafast double ablation in aqueous media for surface enhanced Raman scattering and photonics applications. J. Appl. Phys. **113**, 073106 (2013)
35. K. Kim, S. Choe, Ultrafast nonlinear optical responses of dielectric composite materials containing metal nanoparticles with different sizes and shapes. Plasmonics **12**, 855 (2017)
36. V. Halte, J.-Y. Bigot, B. Palpant, M. Broyer, B. Prével, A. Pérez, Size dependence of the energy relaxation in Ag NPs embedded in dielectric matrices. Appl. Phys. Lett. **75**, 3799 (1999)
37. H. Sanchez-Esquivel, K.Y. Raygoza-Sanchez, R. Rangel-Rojo, B. Kalinic, N. Michieli, T. Cesca, G. Mattei, Ultrafast dynamics in the nonlinear optical response of silver nanoprisms ordered arrays. Nanoscale **10**, 5182 (2018)
38. C.Y. Shih, C. Wu, M.V. Shugaev, L.V. Zhigilei, Atomistic modeling of nanoparticle generation in short pulse laser ablation of thin metal films in water. J. Colloid Interface Sci. **489**, 3 (2017)
39. M. Masnavi, M. Nakajima, K. Horioka, H.P. Araghy, A. Endo, Simulation of particle velocity in a laser-produced tin plasma extreme ultraviolet source. J. Appl. Phys. **109**, 123306 (2011)
40. H. Singhal, R.A. Ganeev, P.A. Naik, A.K. Srivastava, A. Singh, R. Chari, R.A. Khan, J.A. Chakera, P.D. Gupta, Study of high-order

harmonic generation from nanoparticles. J. Phys. B At. Mol. Opt. Phys. **43**, 025603 (2010)
41. R.A. Ganeev, M. Suzuki, M. Baba, M. Ichihara, H. Kuroda, High-order harmonic generation in Ag nanoparticle-contained plasma. J. Phys. B At. Mol. Opt. Phys. **41**, 045603 (2008)
42. C. Rodríguez, Z. Sun, Z. Wang, W. Rudolph, Characterization of laser-induced air plasmas by third harmonic generation. Opt. Express **19**, 16115 (2011)
43. M.L. Naudeau, R.J. Law, T.S. Luk, T.R. Nelson, S.M. Cameron, J.V. Rudd, Observation of nonlinear optical phenomena in air and fused silica using a 100 GW, 1.54 mum source. Opt. Express **14**, 6194 (2006)
44. R.A. Ganeev, H. Singhal, P.A. Naik, J.A. Chakera, M. Kumar, P.D. Gupta, Fourth harmonic generation during parametric four-wave mixing in the filaments in ambient air. Phys. Rev. A **82**, 043812 (2010)